Distribution Agreement

In presenting this thesis as a partial fulfillment of the requirements for a degree from Emory University, I hereby grant to Emory University and its agents the non-exclusive license to archive, make accessible, and display my thesis in whole or in part in all forms of media, now or hereafter now, including display on the World Wide Web. I understand that I may select some access restrictions as part of the online submission of this thesis. I retain all ownership rights to the copyright of the thesis. I also retain the right to use in future works (such as articles or books) all or part of this thesis.

Neil Tramsen April 9, 2021

Attractive and Repulsive Dipolar Interactions in Trilayer Transition Metal Dichalcogenides

by

Neil Tramsen

Ajit Srivastava

Adviser

Department of Physics

Ajit Srivastava

Adviser

Sergei Urazhdin

Committee Member

Dorian Arnold

Committee Member

2021

Attractive and Repulsive Dipolar Interactions in Trilayer Transition Metal Dichalcogenides

by

Neil Tramsen

Ajit Srivastava

Adviser

An abstract of

a thesis submitted to the Faculty of Emory College of Arts and Sciences

of Emory University in partial fulfillment

of the requirements of the degree of

Bachelor of Science with Honors

Department of Physics

2021

Abstract

Attractive and Repulsive Dipolar Interactions in Trilayer Transition Metal Dichalcogenides

By Neil Tramsen

The study of atomically thin monolayer materials has given a unique insight into quantum many-body physics in the past decade, with potential applications in semiconductor devices and quantum information science. Transition metal dichalcogenides (TMDs) have been an area of particular focus in the field, due to their optical properties, which make them ideal photon emitters and detectors, and their lack of inversion symmetry which has opened up the new field of valleytronics [1]. Strong Coulomb interactions lead to excitons, which are tightly bound, optically generated electron-hole pairs that dominate the optical response of TMDs [2]. Interlayer excitons can form in certain TMD heterostructures, with the electron and hole occupying different layers. The resulting charge imbalance creates an electric dipole between layers [3]. Previous work has shown that the resulting dipolar interactions are strongly repulsive, as demonstrated by higher energy biexciton states with an energy increase of around 2 meV [4]. Here, we show that dipole-dipole interactions in TMDs can also be attractive when the dipoles are antiparallel, and by tuning exciton densities confined in moiré potentials we can induce shifts in energy up to 1.5 meV. These findings are a step towards understanding more complicated quantum many-body states that have been predicted for these systems, including exciton lattices and droplets [5, 6]. Furthermore, localized and finely tunable two-state quantum systems represent a major goal in quantum information science [7].

Attractive and Repulsive Dipolar Interactions in Trilayer Transition Metal Dichalcogenides

By

Neil Tramsen

Ajit Srivastava

Adviser

A thesis submitted to the Faculty of Emory College of Arts and Sciences

of Emory University in partial fulfillment

of the requirements of the degree of

Bachelor of Science with Honors

Department of Physics

2021

Acknowledgements

First and foremost, I would like to thank Professor Ajit Srivastava for his unwavering support, insightful teachings and helpful advice throughout my undergraduate degree. I have come a long way since first joining his lab in my sophomore year, and I couldn't have made that journey without him! I would also like to thank Weijie Li, Luka Devenica, and Professor Xin Lu for their assistance and encouragement with my work in the lab. I would like to thank Professor Sergei Urazhdin and Professor Dorian Arnold for their advice and time taken to serve on my committee. I am also grateful to Dr. Alexander Mitrofanov, for his time spent teaching me and working with me on research virtually during the pandemic. Finally, I would like to thank my close friends and family for their endless belief and support.

Contents

1 Introduction **1**

1.1 The band structure of TMDs 2

1.2 Excitons in TMDs 5

1.3 Repulsive dipolar interactions 9

1.4 Model for attractive dipolar interactions in trilayer TMDs 11

2 Methods **15**

2.1 Trilayer sample fabrication 15

2.2 Photoluminescence Spectroscopy 17

2.3 Experimental Procedure 17

3 Results and Analysis **19**

3.1 Characterization of anti-parallel dipolar excitons 19

3.2 Power dependence of interlayer excitons 20

3.3 Effect of moiré potentials on exciton occupations 27

4 Conclusions **31**

5 Outlook **32**

List of Figures

1 Band structure of TMDs 7

2 Repulsive dipolar interactions in bilayer TMDs 10

3 Model for dipolar interactions in trilayer TMDs 14

4 Trilayer sample fabrication 16

5 Optical set up for PL spectroscopy 18

6 Characterization of interlayer excitons 21

7 Energy shifts with power in the $MoSe_2 - WSe_2 - MoSe_2$ trilayer 23

8 Magnetic field splitting 24

9 Energy shifts with power in the $WSe_2 - MoSe_2 - WSe_2$ trilayer 26

10 Ratio of top and bottom interlayer excitons in the $MoSe_2 - WSe_2 - MoSe_2$ trilayer 28

11 Moiré potentials in TMD trilayers 29

12 Shift in energy of exciton peaks with excitation wavelength 30

1 Introduction

Atomically thin "monolayer" materials were thrust into the scientific spotlight in 2004, when Andre Geim and Konstantin Novoselov reported the exfoliation of graphene [8]. Graphene is a one atom thick arrangement of carbon atoms in a honeycomb lattice, previously thought not to exist due to the structure's instability. The discovery resulted in a Nobel prize in 2010, and opened up an entire field dedicated to the study of monolayers produced from van der Waals materials. Graphene has optical, mechanical, and topological properties that had not been seen previously, and mimics the relativistic Dirac equation in a solid state setting [9].

Monolayer materials are made up of 2-dimensional layers stacked on top of each other, with strong covalent bonds within the layer, but comparatively weak van der Waals interactions between layers, holding them together. This makes it easy for the separation of layers and the fabrication of monolayers by mechanical exfoliation [10]. Additionally, different monolayer materials can be stacked to form artificial low-dimensional van der Waals materials with desirable electronic and optical properties [11]. Adding a twist between layers results in unexpected superconducting phases and has led to the new field of "twistronics". [12, 13, 14, 15].

One group of particularly exciting monolayer materials are the transition metal dichalcogenides (TMDs) due to their unique band structure. TMDs are compounds with an atomic structure of MX_2, where M is a transition metal (Mo and W in our samples), and X is a chalcogen (Se in our case). There are a wide variety of different TMD compounds, with

properties such as superconductivity, semi-conducting, semi-metallic and metallic effects [16].

1.1 The band structure of TMDs

Band structures arise in solid materials with a regular atomic structure. One way to understand this band structure is by considering the atomic orbitals in the lattice of atoms. For neighbouring atoms within the lattice, the distance between atoms is small enough for the wave functions of electrons within an atomic orbitals to reach into the neighboring atomic orbital. This lattice can be treated as a regular modulated potential $V(\mathbf{r} - \mathbf{R_i})$, where $\mathbf{R_i}$ represents the lattice vector at the i^{th} atomic site. The potential minima are located at the usual atomic site, and there exists some probability amplitude t that the electron "hops" from one atomic site to another (one potential minimum to the next). The resulting Hamiltonian of such a system is then

$$H_{n,m} = \epsilon_0 \delta_{n,m} - t(\delta_{n+1,m} + \delta_{n-1,m}), \tag{1}$$

where m and n are the m^{th} and n^{th} atomic orbitals on a chain of atoms, and ϵ_0 is the atomic orbital energy. This approach is known as the tight binding method [17], and, upon solving the Schrödinger equation and imposing Bloch's theorem, we find a single band of allowed electron energies with a wavenumber $\frac{-\pi}{a} \leq \mathbf{k} \leq \frac{\pi}{a}$, where a is the interatomic spacing. This band energy is dependent on the electron wavenumber, which in quantum mechanics is proportional to momentum. The wavevectors k of the electron constitute a new lattice in momentum space, called the reciprocal lattice. The most basic cell of this lattice is known as a Brillouin zone, and the Brillouin zone for TMDs is shown in figure 1 (a).

The valence band of a material refers to the lower energy bands of a material, which,

when unaffected by external doping, are filled with electrons. The conduction band is not occupied by electrons in a semiconductor. However, a material can be doped by changing E_F, the fermi energy that defines the occupation of the bands. If the energy is raised high enough, electrons will occupy the conduction band and the material becomes conducting [18]. This is why materials such as TMDs, with fully occupied valence bands, unoccupied conduction bands, and relatively small band gaps, are known as semiconductors.

To calculate the full band structure for a real material, one must also consider all the atoms' orbitals, electron hopping to more than just the nearest neighbouring atom, lattices with more than 1 dimension and multiple lattice vectors, and so on [18]. These calculations are generally completed using computational methods, and figure 1 (b) and (c) show the resulting band structure for WSe_2 and $MoSe_2$ respectively.

The first interesting aspect of a monolayer, semiconducting TMD is the direct band gap in their band structure. As shown in figure 1 (b) and (c), the direct band gap of $MoSe_2$ and WSe_2 is located at the $\mathbf{K}$ (and $-\mathbf{K}$) point of the Brillouin zone. The band gap is "direct" as the valence band maximum and the conduction band minimum is located at the same point in momentum space. This makes it possible to easily excite electrons from the valence band to the conduction band with a photon, which carry comparatively little momentum. The energy band gap is $\Delta E_{gap} = 1.5$ eV for $MoSe_2$ and $\Delta E_{gap} = 1.7$ eV for WSe_2 [19].

To understand further details of a TMDs band structure, we begin with the tight binding model for a hexagonal TMD lattice with a two-atom basis. The two valence band TMD orbitals that mix to form the band structure are the d_{xy} and the $d_{x^2+y^2}$ orbitals, which

have opposite phase at the $\mathbf{K}$ and $-\mathbf{K}$ lattice points, such that

$$\phi_{\pm\mathbf{K}} = d_{xy} \pm i d_{x^2+y^2}, \tag{2}$$

where ϕ indicates the wave function of an electron in the given lattice points. We then form an ansatz solution in the form of

$$\Psi(\mathbf{k}) = \sum_m \frac{e^{i\mathbf{k}R_m}}{\sqrt{N}} \left(C_{\mathrm{A}}(\mathbf{k}) e^{i\mathbf{k}\mathbf{d_1}} \phi_{\mathrm{A}}(\mathbf{r} - \mathbf{R_m} - \mathbf{d_1}) + C_{\mathrm{B}}(\mathbf{k}) e^{i\mathbf{k}\mathbf{d_2}} \phi_{\mathrm{B}}(\mathbf{r} - \mathbf{R_m} - \mathbf{d_2}) \right), \tag{3}$$

where C_A and C_B are the eigenvalues corresponding to the electron state at atom A and B. We have also imposed Bloch's theorem on this ansatz [18], which states that an electron in a periodic potential has eigenstates in the form

$$\Psi^{\alpha}_{\mathbf{k}} = e^{i\mathbf{k}\cdot\mathbf{r}} u^{\alpha}_{\mathbf{k}}(\mathbf{r}). \tag{4}$$

Upon solving the Schrödinger equation $H\Psi = E\Psi$, we find that the eigenvalues of our wavefunction are

$$|\Psi(\mathbf{k} = \pm\mathbf{K} + \Delta)\rangle = \begin{bmatrix} \cos\frac{\theta_{\mathbf{k}}}{2} \\ e^{\mp i\phi} \sin\frac{\theta_{\mathbf{k}}}{2} \end{bmatrix} \tag{5}$$

The phase difference from ϕ comes from the original phase difference between the atomic orbitals at $\pm\mathbf{K}$, which is known as the breaking of inversion symmetry. At the lattice points $\mathbf{K}$ and $-\mathbf{K}$, $\phi = 0$. However, as we move away from the lattice point, ϕ has a non-zero value and results in a pseudo-spin in the electron's wave function. This spin is opposite at $\pm\mathbf{K}$, and needs to be conserved when an electron is excited from the valence band into the conduction band. The difference in spin is ± 1 at $\pm\mathbf{K}$, and this angular momentum can be provided by circularly polarized light. As a result, electrons in the $\mathbf{K}$ being excited by right-hand circularly polarized light (σ_-) and electrons in the $-\mathbf{K}$ being excited by left-hand

circularly polarized light (σ_+). This is known as the valley degree of freedom, and allows precise control over the exciton states excited, and also makes it possible to measure the state by probing the helicity of the emitted photons, opening up the field of "valleytronics". The valley degree of freedom is also shown schematically in 1 (d).

Another important detail of this band structure is the band splitting due to spin orbit coupling (SOC). Einstein's theory of special relativity describes how electric and magnetic fields behave in different reference frames, and in the reference frame of a moving electron, the changing electric field due to the periodic potential acts as a magnetic field. This magnetic field shifts the energy of electrons depending on their spin (spin up or down in the z-basis), resulting in two distinct bands. In TMDs, this splitting is on the order of 10 - 100 meV, with a greater splitting in the valence band than the conduction band. For an example, in WSe_2, the splitting in the valence band is around $\Delta E_{SOC} = 450$ meV, whereas in the conduction band the splitting is only around $\Delta E_{SOC} = 40$ meV [20]. The direction of the field depends on the direction of change of the electric field, and so the SOC-induced change in energy is opposite at the $\mathbf{K}$ and $-\mathbf{K}$ lattice points, as shown in figure 1 (d).

1.2 Excitons in TMDs

The excitation of electrons from the valence band to the conduction band results in the formation of a quasi-particle known as an exciton. The negatively charged electron leaves behind a vacancy in the valence band, resulting in a net-positively charged gap known as a hole. The negatively charged electron is attracted to the positively charged hole by the coulomb interaction, resulting in a bound state [21]. The exciton is charge neutral, as the

electron has a charge of $-e$, and the hole has a net positive charge of $+e$. In WSe_2, excitons generally have a lifetime on the order of picoseconds [22], before the electron drops back down to the energetically favourable valence band and recombines with the hole, emitting a photon that can then be measured. The exciton remains localized in one layer, and is therefore known as an intralayer exciton. This quasi-particle has its own band structure which is calculated from the band structure of the electron and hole.

So far, we have only discussed the electronic properties of monolayer TMDs. The picture gets more complicated when multiple monolayer TMDs are stacked on top of one another. Different TMDs have different energy bands band gaps. In this case, WSe_2 and $MoSe_2$ band gaps are arranged as shown in figure 1 (e), where the $MoSe_2$ bands are at lower energies than the WSe_2 bands. This particular alignment is known as type-II band alignment. For an exciton excited in WSe_2, it is energetically favourable for the hole to be in WSe_2, and for the electron to be in the $MoSe_2$ layer. As a result, the hole will move into the WSe_2 layer, through a process known as quantum tunnelling [23].

The resulting interlayer excitons have a significantly longer lifetimes (nanoseconds) than intralayer excitons (picoseconds) [3]. Furthermore, they induce a spatial charge imbalance between the two layers, as the negatively charged electron is in one layer, and the positive charge associated with the hole is in another layer. An electric dipole is formed between the two layers, going from the negative electron to the positive electron. The dipole moment, p, is

$$p = e \cdot d, \tag{6}$$

where e is the electronic charge, and d is the separation of the two charges. For excitonic

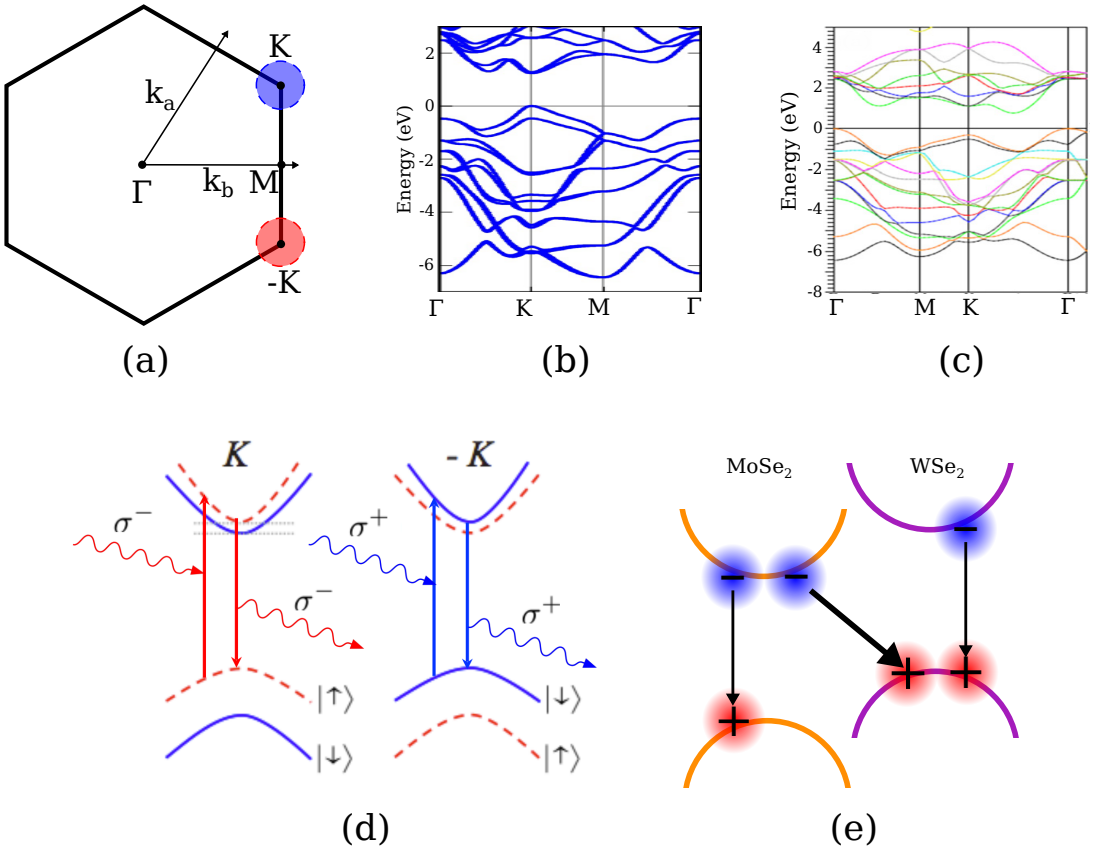

Figure 1: Band structure of TMDs. (a) Brillouin zone of a TMD, showing the unit cell of the atomic lattice in momentum space. Highlighted are the K and −K points at which TMDs have a direct band gap. (b) Band structure of WSe_2, showing the direct band gap at the K lattice point. Adapted from reference [20]. (c) Band structure of $MoSe_2$, again showing the direct band gap. Adapted from reference [24]. (d) Electron excitation at the **K** and $-\mathbf{K}$ lattice points due to TMD valleys and SOC. Spin up electrons are excited at the **K** point with σ_-, whereas spin down electrons are excited at $-\mathbf{K}$ with σ_+. (e) Formation of interlayer excitons between WSe_2 and $MoSe_2$ bands, with type II band alignment.

dipoles, we expect a layer separation of 0.7 nm, giving them a dipole moment of 0.7 nm·e.

To understand the effect of an electric field on this dipole, we must first understand the structure of the sample. Voltages can be applied across the sample using a top gate and a bottom gate. In our sample, the top gate is made of a thin sheet of graphite placed above the sample, and the bottom gate is the heavily doped silicon substrate the sample is fabricated on. Two layers of hBN are placed between the gates and the sample, to insulate it from the conducting sheets. The sample is also insulated from the silicon by a layer of SiO_2 ($\sim$300 nm thick). We can treat this sample as a capacitor, with the two gates acting as parallel plates, and everything in between being the dielectric. The electric field in the sample is given by

$$E_s \approx \frac{\epsilon_i}{\epsilon_s}\frac{\Delta V}{d}, \tag{7}$$

where E_s is the electric field in the sample, ϵ_s is the permittivity of the sample (the permittivity of $MoSe_2$ and WSe_2 is $\epsilon_s = 7.4\epsilon_0$ [25]), ϵ_i is the dielectric constant of the insulators ($\epsilon_{hBN} \approx \epsilon_{SiO_2} = 3.5\epsilon_0$ [26]), ΔV is the voltage across the entire sample, and d is the thickness of the entire sample. This equation is approximate as it assumes the thickness of the sample is small compared to the insulating materials. Finally, the change in energy of the dipolar excitons in response to the electric field is

$$\Delta U = -p \cdot \Delta E_s. \tag{8}$$

The exact composition and fabrication of the sample is described in section 2 and figure 4.

To detect excitons, we can measure the photons emitted by the recombination of the electron and the hole in a charge-coupled device (CCD). At low powers, we often see

excitons in the form of quantum dots, which are excitons trapped in narrow potentials due to lattice impurities or potentials induced by multiple lattices (moiré potentials) [27]. At higher powers, we also see a broad peak, which is a result of excitons having more spatial freedom and existing at higher densities.

1.3 Repulsive dipolar interactions

Our research group has previously shown that repulsive interactions occur between dipolar interlayer excitons, represented schematically in figure 2 (a). A heterobilayer TMD sample was fabricated, made of a WSe_2 and a $MoSe_2$ monolayer. Dipolar interlayer excitons formed between the two layers, as confirmed by electric field scans, which caused the dipole's energy to shift with the electric field (figure 2 (b)). Repulsive interactions occurred between excitons in highly localized quantum dots, which confine the excitons to small potentials (see schematic in figure 2 (a)). As the incident laser power was increased, the dipolar excitons formed biexcitons [4]. In figure 2 (c) IX1 is the exciton, and IXX1 is the biexciton. These states can be seen jittering together due to the interaction between the two dipoles. The repulsive interaction results in a 2 meV increase in energy. Figure 2 (d) shows the increase in probability of biexciton states at higher incident laser powers.

In monolayer TMDs, the bound biexciton state usually results in a reduction in energy [28]. However, due to repulsion between dipoles, this state actually resulted in an increases in energy in the bilayer case. It was also determined that the biexciton was made up of an exciton from each Brillouin zone ($\mathbf{K}$ and $-\mathbf{K}$), as this state minimized the exchange energy of the excitons [4].

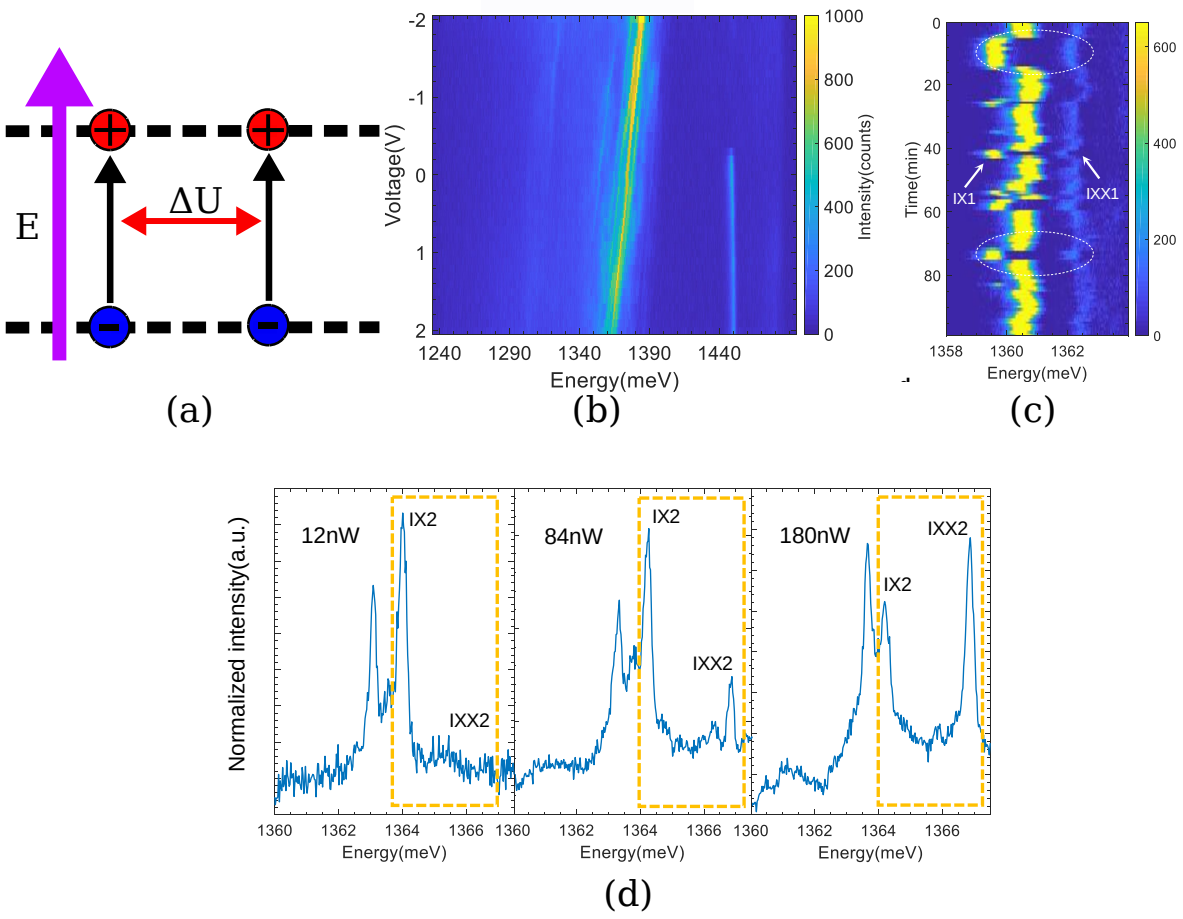

Figure 2: Repulsive dipolar interactions in bilayer TMDs. (a) Repulsion between two dipolar excitons in a heterobilayer TMD. (b) Shift in energy of dipolar exciton PL with electric field. The shift is approximately 1.5meV. (c) Correlated jittering between exciton and biexciton states. (d) Intensity of biexciton peak with increasing power. As power increases, the intensity of biexciton emission increases. Figures (b)-(d) adapted from reference [4].

Having confirmed that dipolar interactions between interlayer excitons led to repulsion between excitons in heterobilayer TMDs, we posed the question of whether this interaction could also lead to attraction between excitonic dipoles. Attractive dipolar interactions have previously been seen in GaAs quad-layer structures [29], and predicted in trilayer TMDs [5], but experimental evidence in TMDs has remained elusive. Attraction between dipoles in monolayer TMDs could open the door to new phases of matter, including exciton droplets, and allow us to develop our understanding of quantum many-body states in these materials [6]. Interactions between electric dipoles can be attractive when the dipole moments are in opposite directions (antiparallel). However, in bilayer samples, the electrons and holes are always in the same layer, resulting in dipolar excitons that are always in the same direction. The only way to generate antiparallel electric dipoles is to fabricate a sample with more TMD monolayers. To achieve this, we proposed the fabrication of a trilayer sample, as described in the next section.

1.4 Model for attractive dipolar interactions in trilayer TMDs

Antiparallel dipoles can form in trilayer TMD heterostructures, as shown in figure 3 (a). For an exciton formed in the middle WSe_2 layer, the electron can tunnel to either the top or the bottom $MoSe_2$ layer to minimize its energy. To calculate the expected energy of interacting exciton dipoles in a trilayer TMD sample, we will begin with the simplest model: the charges in two antiparallel excitons. There are two repulsive interactions between the electrons and the electron holes, and two attractive interactions between the two electron-hole pairs (see figure 3 (b) inset). We do not consider the intrinsic electron-hole attraction, as this is a part

of the bound exciton. Using this simple model, the energy as a function of r, the distance between the two excitons, is

$$E(r) = e^2 k \left(\frac{1}{r} + \frac{1}{\sqrt{r^2 + 4d^2}} - \frac{2}{\sqrt{r^2 + d^2}} \right). \tag{9}$$

The resulting energy is shown in figure 3 b).

To build on this primitive model and develop a more precise approximation of the energy for our system, we consider 3 large, 2-dimensional planes, in which excitons are excited at a constant density between planes. A schematic of this model is shown in figure 3 (c). To model the system, we perform a mean-field calculation for a constant density of excitons.

There are two dipolar exciton densitities we must concern ourselves with: the density in the top layer and in the bottom later, given by nT and nB. We calculate the effect of this field of excitons on a sample exciton that is being added to the field. The total energy is found by intergrating over the two fields such that

$$\Delta U = U^{\text{intra}} + U^{\text{inter}} \tag{10}$$

$$U^{\text{inter}} = 2\pi e^2 k \int_{r_0}^{\infty} r \left(\frac{1}{r} + \frac{1}{\sqrt{r^2 + 4d^2}} - \frac{2}{\sqrt{r^2 + d^2}} \right) n_T dr \tag{11}$$

$$U^{\text{intra}} = 2\pi e^2 k \int_{r_0}^{\infty} r \left(\frac{2}{r} - \frac{2}{\sqrt{r^2 + d^2}} \right) n_B dr. \tag{12}$$

In this system, the starting point of the integral, r_0, is the distance to the closest exciton, which shrinks as the density increases. Therefore, we set $r_0 = \frac{1}{\sqrt{n}}$. Solving these equations for values of n_T and n_B, we generate the phase space in figure 3 (d). There exists an attractive region for an exciton inserted into the top layer when the ratio of densities is $\frac{n_T}{n_B} < 1$. For

ratios of $\frac{n_T}{n_B} > 1$, the interaction becomes repulsive, as shown in the corresponding line graphs in figure 3 (e). This means that, for attractive interactions to be measured, we need to find a region in a trilayer sample where the ratio of top-layer dipoles to bottom-layer dipoles is less than 1. Significant attractive interactions should be observed at ratios of around 2:1.

The usefulness of these equations relies largely on our ability to determine n_T and n_B. We are able to measure the excitation power used to excite electrons and form excitons, as well as the resulting intensity from the recombination of excitons. The intensity of photon emissions can be written as

$$I = c\frac{\rho_{IX}}{\tau_{IX}}, \tag{13}$$

where ρ_{IX} is the probability of finding an electron in an exciton state, τ_{IX} is the exciton lifetime of excitons, and c is a constant of proportionality. The probability ρ_{IX} is directly proportional to the exciton density, and as a result, intensity is too. This makes sense, because intensity increases as the number of excitons recombining per seconds has increased, which means that the total number of excitons has increased. Therefore we only need to determine the total intensity of top and bottom dipolar excitons to determine the parameters n_T and n_B used in equations 10 - 12. The exact density can be calculated from intensity as

$$n = \frac{1}{c}\frac{I\tau_{IX}}{t_{int}A_l}, \tag{14}$$

where τ_{IX} is the lifetime of an interlayer exciton, c is the percentage of photons that are actually detected by the detector, t_{int} is the integration time, and A_l is the area of material excited by the laser.

One important detail to consider is that the excitons are not free to arrange them-

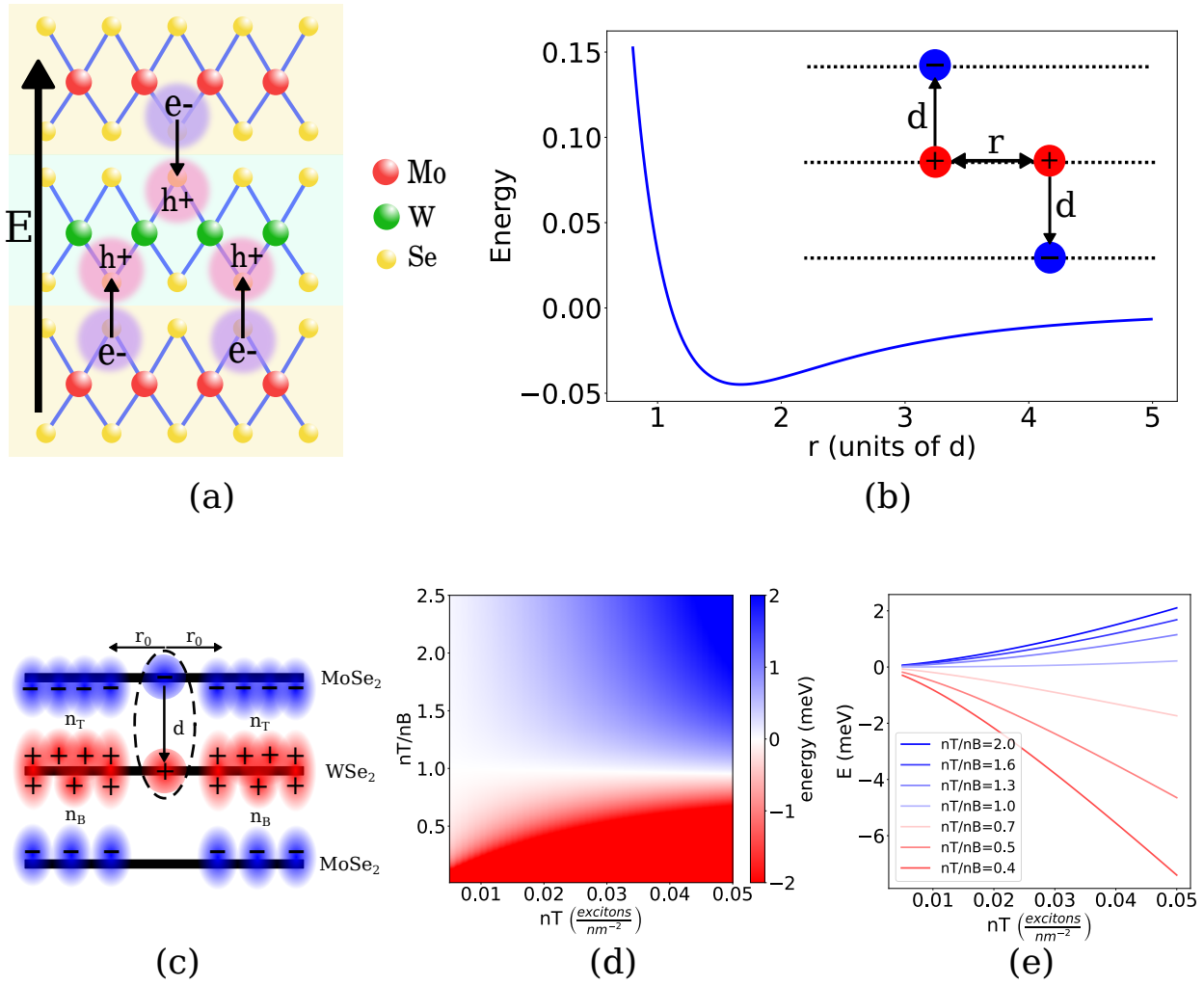

Figure 3: Model for dipolar interactions in trilayer TMDs. (a) Atomic arrangement of trilayer TMD, showing formation of interlayer excitons. (b) Energy of dipole-dipole interaction between two excitons, see inset. (c) Model for mean-field calculation, showing densities of top and bottom dipolar excitons. (d) Phase space of dipolar interaction energy with density and ratio of top and bottom excitons. Attractive region (red) exists when the ratio of exciton densities is $\frac{n_T}{n_B} < 1$. (e) Line graph of interaction energies, showing attractive and repulsive regions for given exciton densities and ratios.

selves such that their energy is minimized in an attractive arrangement. Interlayer excitons are confined to potentials known as moiré potentials, which are a result of the stacking and mixing of the potentials of multiple lattices [30]. Moiré potentials will be discussed more carefully in section 3.2, as they have a significant effect on the results we see.

It should be noted that we use the above model to justify that attractive potentials can, and should, exist between interlayer excitons, when they interact at certain densities. While being easy to understand, this model does not provide the full picture of the highly complicated quantum interactions that take place within the TMD lattices, and will therefore not predict the exact energies of interlayer excitons, as is discussed in section 3.

2 Methods

2.1 Trilayer sample fabrication

TMD monolayers were mechanically exfoliated from the bulk crystal using tape to peal off thin layers. Layers were then transferred from the tape onto a 300 nm SiO_2/Silicon substrate, and monolayers were identified using an optical microscope. Atomic force microscopy was used to confirm the thickness of monolayers, which is around 0.7 nm. A slide is prepared with an area of curved polydimethylsiloxane (PDMS) to pick up monolayers from one silicon slide and transfer them to another, stacking them in the desired arrangement. Using this method, two samples were created, one with a $MoSe_2 - WSe_2 - MoSe_2$ arrangement, and a second sample with a $WSe_2 - MoSe_2 - WSe_2$ arrangement. Both samples allow us to test our hypothesis, with the dipoles expected to be in opposite directions in the two samples,

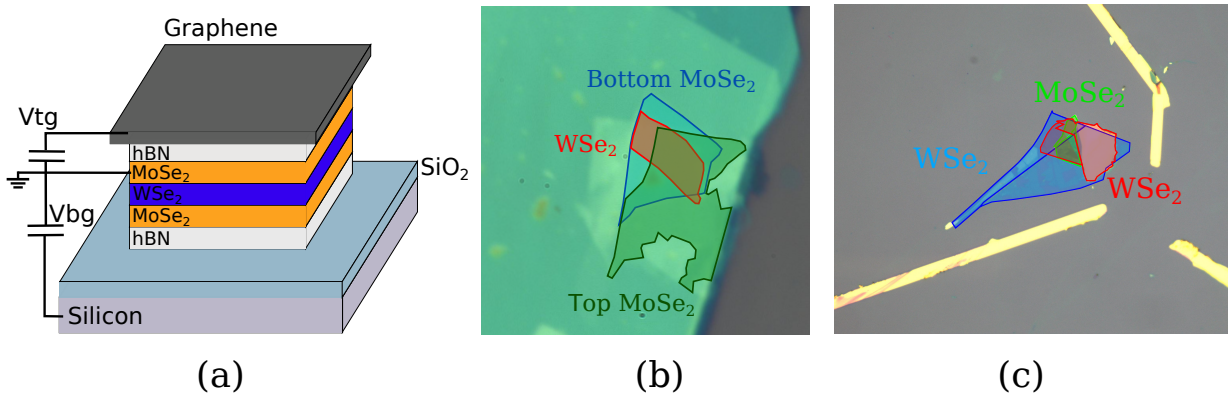

Figure 4: Trilayer sample fabrication. (a) Schematic of the full trilayer sample arrangement, showing electric field controls and substrates. (b) Image of $MoSe_2 - WSe_2 - MoSe_2$ sample. (c) Image of $WSe_2 - MoSe_2 - WSe_2$ sample.

due to the inversion of the monolayer order.

A thin layer of graphite was added above the monolayers, acting as an electric contact to control the voltage across the sample. The silicon substrate slide was used as the lower contact. Thin pieces ($\sim$ 40 nm) of hBN were placed between the monolayers and the graphite contacts, insulating the sample from contacts. This arrangement allows us to precisely control the electric field across the sample with the hBN and sample acting as a dielectric between the two pieces of graphene, acting as a capacitor. The sample itself also has an electric lead connected to it, allowing it to be grounded. These leads are connected to voltage supplies using wire bonding. The final arrangement is shown in Figure 4 (a), along with images of the two fabricated samples in Figure 4 (b) and (c).

2.2 Photoluminescence Spectroscopy

The optical set-up for measurement is shown in Figure 5. The first cryostat used is a closed-cycle cryostat (AttoDry 800), which is cooled to around 4K. The second cryostat (BlueFors Cryogenics) has a built-in superconducting magnet, with magnetic field capabilities from -8 to 8T. This cryostat is also cooled to around 4K. A piezoelectric controller (Attocube Systems) is used for precise control over the position of the sample within the cryostat. The Ti:Sapphire tunable laser allows close control of the excitation wavelength, with a tunable wavelength range of 700nm to 1000nm, whereas the HeNe laser has a wavelength of 632.8nm. The incident polarization is controlled using a polarizer and a liquid crystal retarder (LCR), which has a variable retardance. This variable retardance is controlled by applying a voltage across the liquid crystal, which rearranges itself and changes the retardance on the principal axis. Emitted photons are collected in a charge coupled device (CCD) (Princeton Instrument HR-500 for AttoDry 800 and Princeton Instruments SP-2750i for BlueFors cryogenics). Emission can also be resolved by polarization using a Wollaston prism which separates horizontally polarized light from vertically polarized light. A $\lambda/4$ retarder is used to convert the emitted circularly polarized light to linearly polarized light, which can then be measured using polarizers.

2.3 Experimental Procedure

The fabricated samples were loaded into the two cryostats, and cooled down to 4K. The lasers were used to excite electrons in the sample, with our optical bench allowing us to use any light source interchangeably. A large portion of the equipment can be controlled remotely

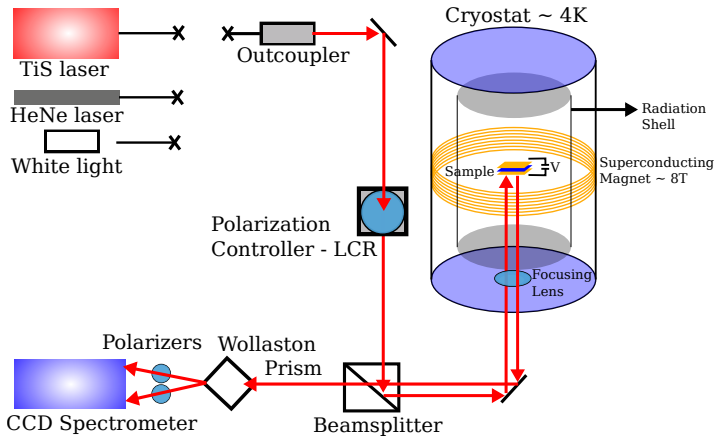

Figure 5: Optical set up for PL spectroscopy.

through MATLAB and other computer scripts. However, manual checks and adjustments are required in every experiment to ensure the data's quality, and to adjust the equipment that cannot be remotely controlled.

We then performed a series of experiments on each sample. Voltage scans were performed by applying a potential difference across the sample, using the prefabricated contacts. This induced an electric field across the sample. Power scans were performed by increasing the power of the laser incident on the sample. This increases the number of photons hitting the sample per second. The superconducting magnet in the cryostat is used to apply a magnetic field perpendicular to the sample. Photoluminescent excitation (PLE) experiments require changing the excitation wavelength, and the TiS laser can be used for this purpose. Changing the excitation wavelength can change the efficiency at which excitons are created in the sample.

For each experiment, photons emitted by the sample are collected in the CCD, giv-

ing us information about the intensity at each wavelength. We also have precise control over the incident polarization, allowing us to shine left-hand and right-hand circularly polarized light on the sample. We can resolve between these two circular polarizations in the collected photons too. Using these processes, we collected the data in section 3.

3 Results and Analysis

3.1 Characterization of anti-parallel dipolar excitons

We begin by confirming the existence of dipolar excitons in the PL from the trilayer region of the sample. Figure 6 (a) shows the shift in energy of quantum dots with voltage. We see primarily red-shifting dipoles (decreasing in energy) between 900 and 970 nm, and primarily blue shifting dipoles (increasing in energy) between 970 and 1000 nm, as the voltage across the sample increases. From figure 3 (a) we assign the red-shifting peaks as top dipoles, and blue-shifting peaks as bottom dipoles in the $MoSe_2 - WSe_2 - MoSe_2$ trilayer. We estimate the electric field to be $1.8 \times 10^7 \mathrm{Vm}^{-1}$ at -15 V from equation 7, and for a ΔV of 15V, we expect a shift in exciton energy of 12 meV. This corresponds closely to the observed shift in figure 6 (a) of around 15 meV over 15 V, with the main source of uncertainty in equation 7 being the sample thickness.

Figure 6 (b) shows the jittering of these dipolar peaks over time, and provides further evidence of the opposite dipoles. Jittering is caused by small fluctuations in the local electric field of the sample. As shown, there is an opposite correlation in the long-term drifting of peaks. This is because these shifts in electric field have an opposite effect on the

two antiparallel dipoles, resulting in equal and opposite energy changes.

Figure 6 (c) shows the photoluminescent excitation (PLE) emissions for varied excitation energy. There are two resonances at which the intensity of emission is significantly amplified, one at around 725 nm and another at around 770 nm. These resonant wavelengths correspond exactly to the resonant frequencies for excitons excited in monolayer WSe_2 and $MoSe_2$ respectively [31]. The dipolar excitons in the trilayer sample show both resonances, as excitons can be excited in either layer and then tunnel to form an interlayer exciton. Interestingly, the $MoSe_2$ resonance is significantly stronger than the WSe_2 resonance in this particular sample.

3.2 Power dependence of interlayer excitons

Having confirmed the existence of both top and bottom dipoles, with behaviour exactly as expected, we proceed with a set of power dependence experiments to confirm the relationship proposed in section 1.4, the results of which are shown in figure 7. We observed significant shifts in energy of all dipolar excitonic peaks in the $MoSe_2 - WSe_2 - MoSe_2$ sample, as shown in figure 7 (a). These shifts were present when increasing the power, and shifted back almost exactly equally when reducing the power back to its original value, as shown in figure 7 (b), meaning that this was not a jittering or drift effect, instead being truly dependent on power. The shifts in energy varied from peak to peak, with the largest redshift observed being around 1.5meV, while the largest blue shift observed was only around 0.5meV.

We classified the peaks that shift with power into top and bottom interlayer excitons using further voltage scans, the results of which are shown in figure 7 (c). This figure clearly

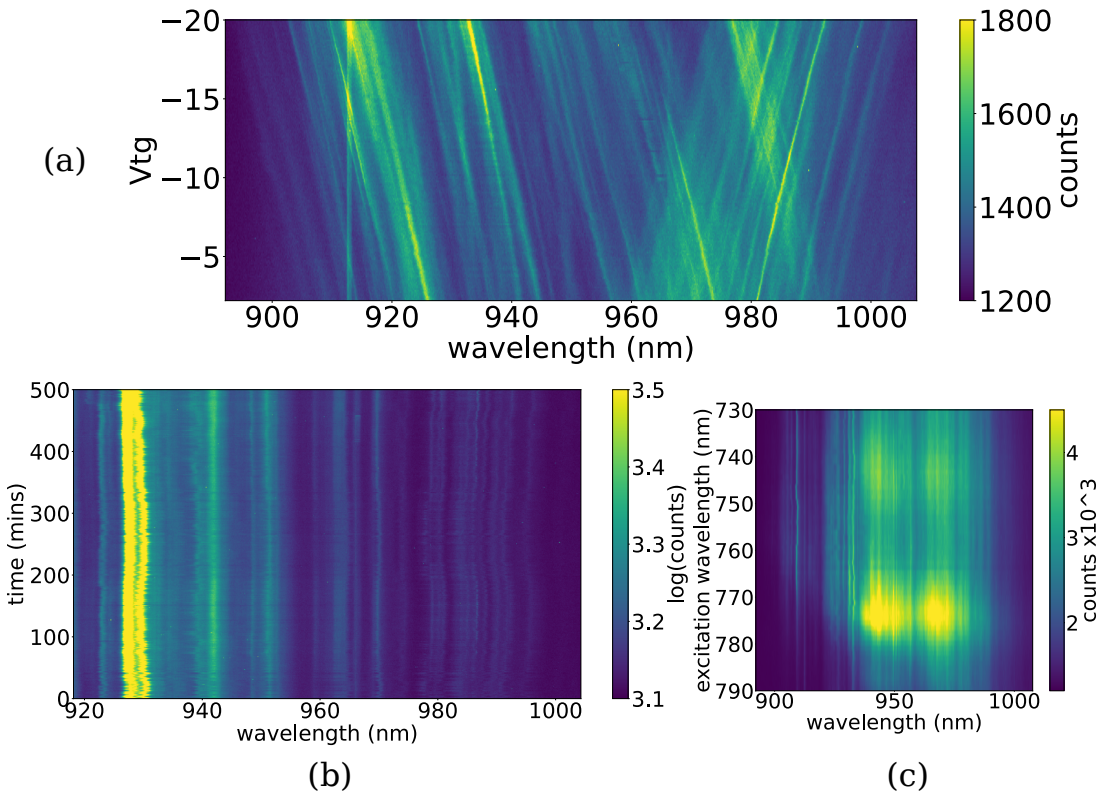

Figure 6: Characterization of interlayer excitons. (a) Shift in energy of dipolar excitons with electric field. We see a shift of around 15meV over 15V, which corresponds closely to the predicted value (excitation wavelength=720 nm, integration time=40 s). (b) Dipolar exciton jittering, showing anti-correlated drift due to the antiparallel dipoles (excitation wavlength=771 nm, V=-20V, integration time=50 s, excitation power=1 μW). (c) PLE in the trilayer region, showing PLE resonances for both $MoSe_2$ and WSe_2 (excitation power= 20 μW, V=-40 V, integration time=40 s).

shows that the peaks that red-shift with power are the top excitons, whereas the bottom excitons blue shift with power. However, the intensity of the top excitons is significantly stronger than the bottom excitons, suggesting that the ratio $\frac{n_T}{n_B}$ is greater than 1 (which is confirmed in figure 10. This directly conflicts with the calculations made in figure 3 (d), which clearly showed that red-shifts with power would only be expected for ratios of $\frac{n_T}{n_B} < 1$.

The shifts in power are even more clearly visible under a magnetic field (B), for which we can calculate the degree of circular polarization (DCP). As discussed in section 1.1, the bands of $MoSe_2$ and WSe_2 exhibit both SOC and emission with opposite circular polarization at opposite valleys due to inversion symmetry breaking. This means that, when applying B, the energy peaks split into two due to SOC, and one peak emits σ_+ while the other emits σ_-. This splitting is shown in figure 8 (a) and is clearly visible in the DCP, which calculates the ratio of $\sigma+$ to $\sigma-$ as

$$DCP = \frac{\sigma_+ - \sigma_-}{\sigma_+ + \sigma_-}. \tag{15}$$

From this data we also calculated the g-factor, using the regression shown in figure 8 (b). The g-factor is the effective magnitude of spin of the excitons [32], and is given by

$$E_{\sigma_+} - E_{\sigma_-} = g\mu_B B, \tag{16}$$

where $E_{\sigma_+} - E_{\sigma_-}$ is the energy splitting induced by B, and μ_B is the Bohr magneton. In our sample, we found that $g = 7.0 \pm 0.7$, which matches closely to previous results for layers with small twist angles (1^o in our sample) [33]. Finally, the DCP shows clear shifts in the energy of top and bottom peaks with power, as shown in figure 8 (c). This can be particularly useful when there is a lot of background noise, with the DCP making peaks clearly visible.

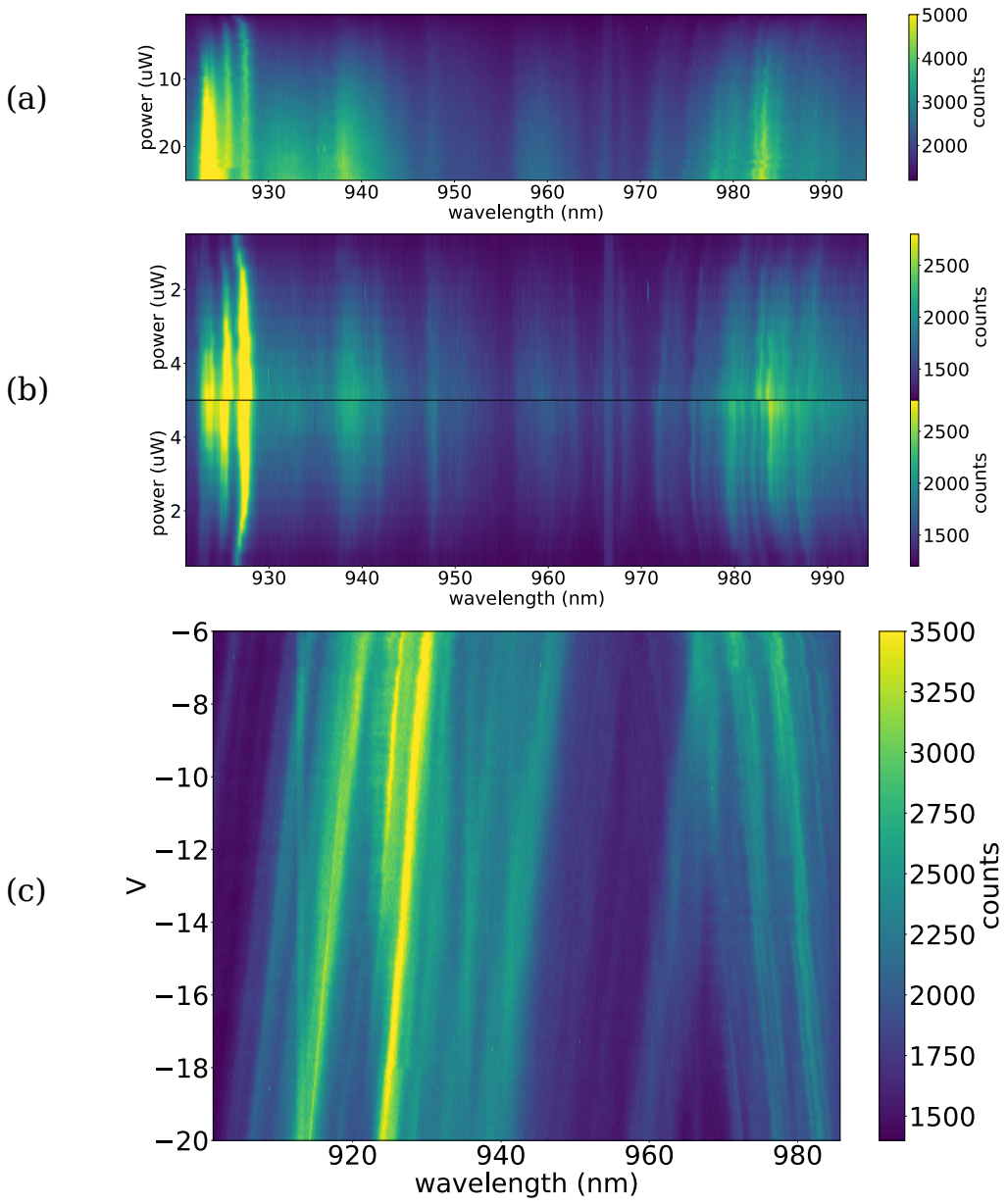

Figure 7: Energy shifts with power in the $MoSe_2-WSe_2-MoSe_2$ trilayer. (a) Region showing red and blue shifts with power. The greatest red shift were around 1.5meV, while blue shifts were around 0.5meV (excitation wavlength=633 nm, inegration time=100 s, V=-20 V). (b) Detail on both increase and decrease in power from 0 to 5 μW, showing the reversibility of the shifts. (c) The corresponding peaks shifting with electric field, signalling the direction of the dipole.

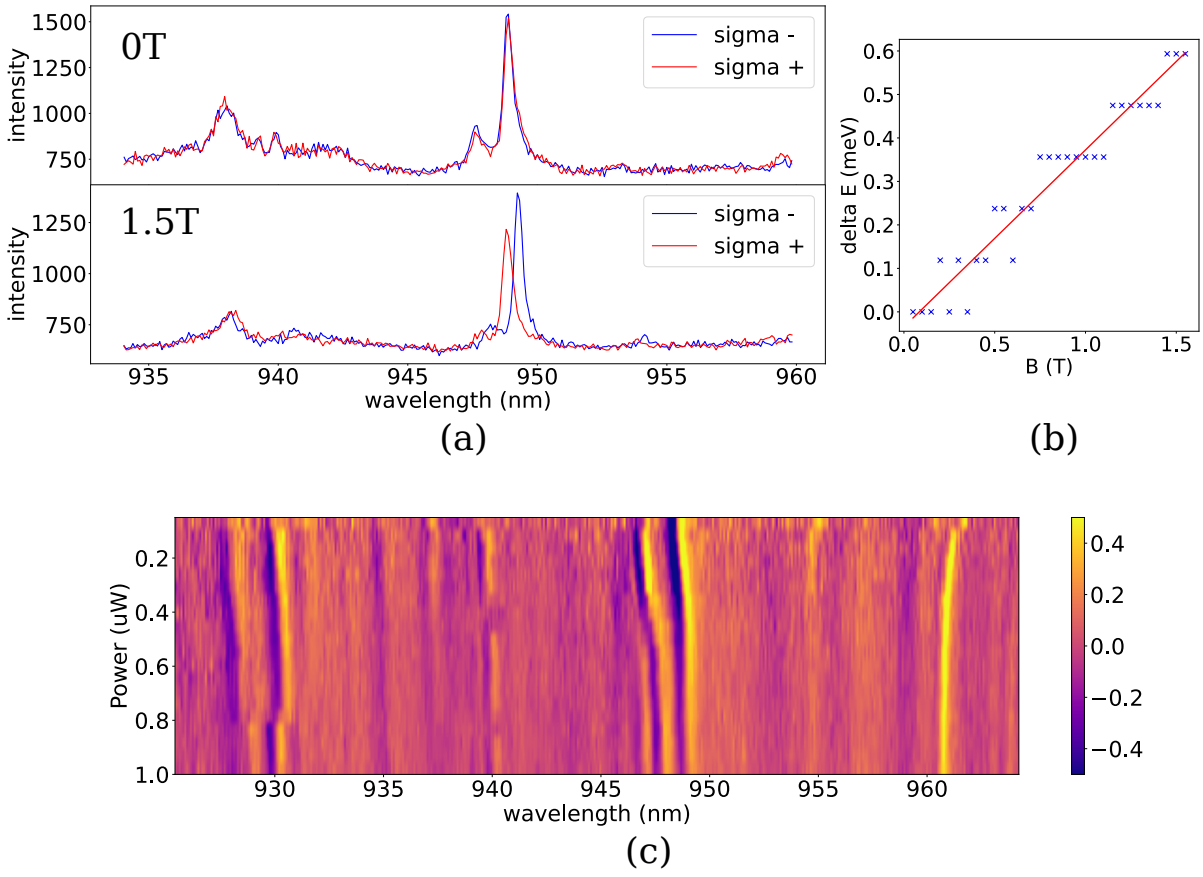

Figure 8: Magnetic field splitting. (a) Exciton peak splitting at 0T and 1.5T (excitation wavelength=735 nm, excitation power=20 μW, integration time=50 s). (b) Least squares regression of energy splitting with B-field, with g = $7.1\mu_B \pm 0.7$. (c) DCP of power dependence at 1.5T, showing clear shifts over the background due to magnetic field splitting.

We tried to further confirm our findings by repeating the power dependence measurements on our second sample, a $WSe_2 - MoSe_2 - WSe_2$ trilayer. Red shifts were seen in this sample too, with the power dependence data is presented in figure 9. In 9 (a) we see an overview of the power dependence, which features a bright and broad exciton peak. The broad peak is a result of the higher powers and a shallower potential, meaning that excitons have more freedom in momentum. Peaks are again assigned to top and bottom peaks using a voltage scan, shown in 9 (b). Figure 9 (c) shows the red shift observed, which is around 1.5 meV.

Overall, the second sample proved much more difficult to investigate, and this is reflected in the quality of the data. Almost all the obvious shifts were blue shifts, and red shifts proved difficult to locate. We did eventually find the red shift shown in figure 9 (c), however the peak is much weaker compared to the first sample. Due to small changes in the twist angles between monolayers, strain in the monolayers, and other small inaccuracies in the fabrication process, it is not unusual for each sample to exhibit slightly different properties.

The red shift seen in the second sample is around 1.5meV, however, as seen in the figure the peak is much weaker, and generally the sample data is of lower quality, with fewer localized quantum dots. This is a reminder of the fact that in this field, each new sample will often exhibit slightly different characteristics, and it is the fine control of these characteristics that is one of the long term goals. While the shifts were harder to detect in this sample, they were still present, suggesting the attractive interaction is taking place once again.

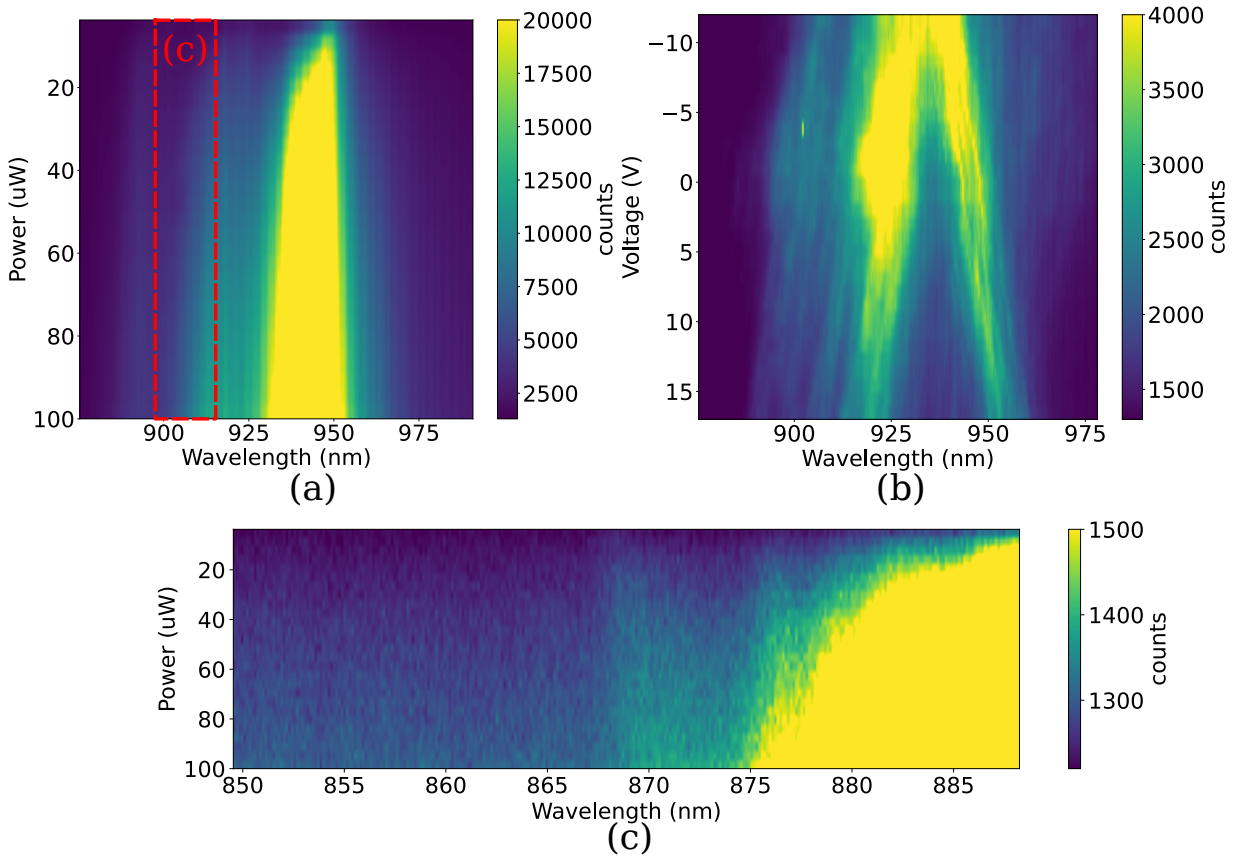

Figure 9: Energy shifts with power in the $WSe_2 - MoSe_2 - WSe_2$ trilayer. (a) Region showing red and blue shifts with power, and a broad exciton peak in the center (excitation wavelength=633 nm, integration time=100 s). (b) Exciton peak shifts with voltage, showing that peaks ¡940 nm are bottom peaks in this sample, and peaks greater than 940 nm are top peaks. (c) Red shift in exciton peak with power, signifying dipolar attraction.

Figure 10 shows the integrated intensity of each dipole in figure 7 (a). From the integrated intensities we see that the ratio $\frac{n_T}{n_B} \approx 2.5$ (figure 10 (b)) remains relatively constant with power after a small initial increase. This means that the generation rate for both top and bottom interlayer excitons remains relatively constant, and the interlayer excitons are not saturating. However, this ratio directly conflicts with the model proposed in section 1.4, in which it was shown that the ratio had to be $\frac{n_B}{n_T} < 1$ for the attractive minima that we were hoping to observe (figure 3 (d)). This is similar in the second sample. From figure 9 (b) we see that the ratio of dipoles $\frac{n_T}{n_B}$ is closer to 1 than in the first sample, however the red shifting bottom peaks still have a higher densities than the blue shifting top peaks. Indeed, the simple mean field calculation does not capture the full picture. In particular, it does not capture the previously mentioned moiré potentials, which significantly impact the spatial distribution of interlayer excitons.

3.3 Effect of moiré potentials on exciton occupations

Figure 11 (a) shows the expected moiré potential landscape for two excitons in a trilayer heterostructure with twist angles of 2^o and 3^o between layers. In our sample, we expect twist angles of $\approx 1^o$, however the resolution of our microscope limits the resolution of the twist angle. The size of potential wells is proportional to $\frac{1}{\theta}$ for small twist angles, where θ is the twist angle. This means that a doubling in the angle halves the size of the moiré potential, and results in the structure shown. Figure 11 (b) shows these potentials for just the electron, and shows how maxima are surrounded by multiple minima. This results in the picture shown in figure 11 (c), where each moiré potential trapping a top exciton is surrounded

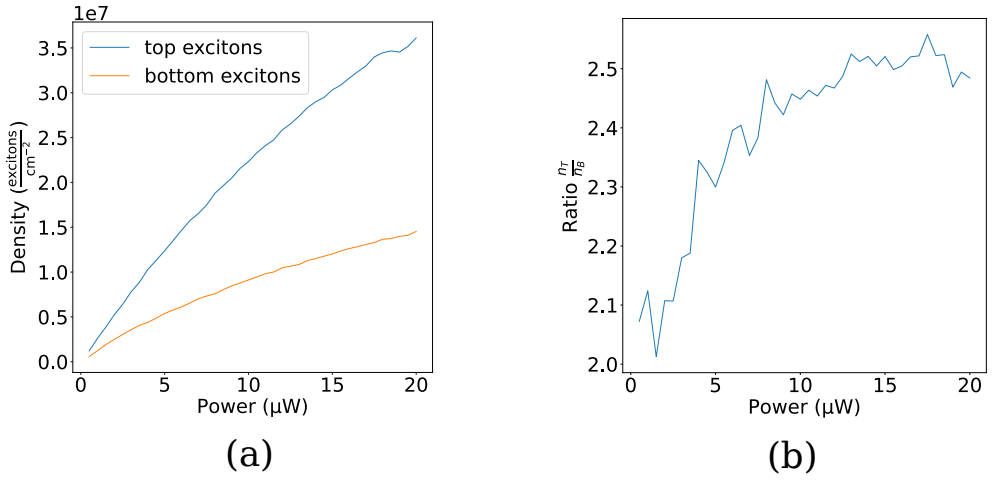

Figure 10: Ratio of top and bottom interlayer excitons in the $MoSe_2-WSe_2-MoSe_2$ trilayer. (a) Integrated intensities from figure 7 (a). (b) Ratio of top dipoles to bottom dipoles as a function of power. There is an initial increase in the ratio, which then flattens at 2.5 suggesting that the generation rate of both dipoles becomes constant.

by multiple moiré potentials trapping bottom excitons [30]. This means that, despite the intensity of top excitons being stronger in our sample, they are locally surrounded by multiple potentials of bottom excitons. As the occupation of both potentials increases with power, the top excitons red shift due to their proximity to more bottom excitons, whereas the bottom excitons blue shift as their small potentials are close to other small potentials of bottom excitons. Therefore, the model proposed in 3 holds when considering the local moiré structure which really controls the densities of local excitons, and the interactions between them. The observed intensity of exciton emissions can also be signifcantly affected by moiré potentials, suggesting that the calculated density may also need to account for the twist angle between layers [34].

One interesting effect that may provide further insight into the confinement of

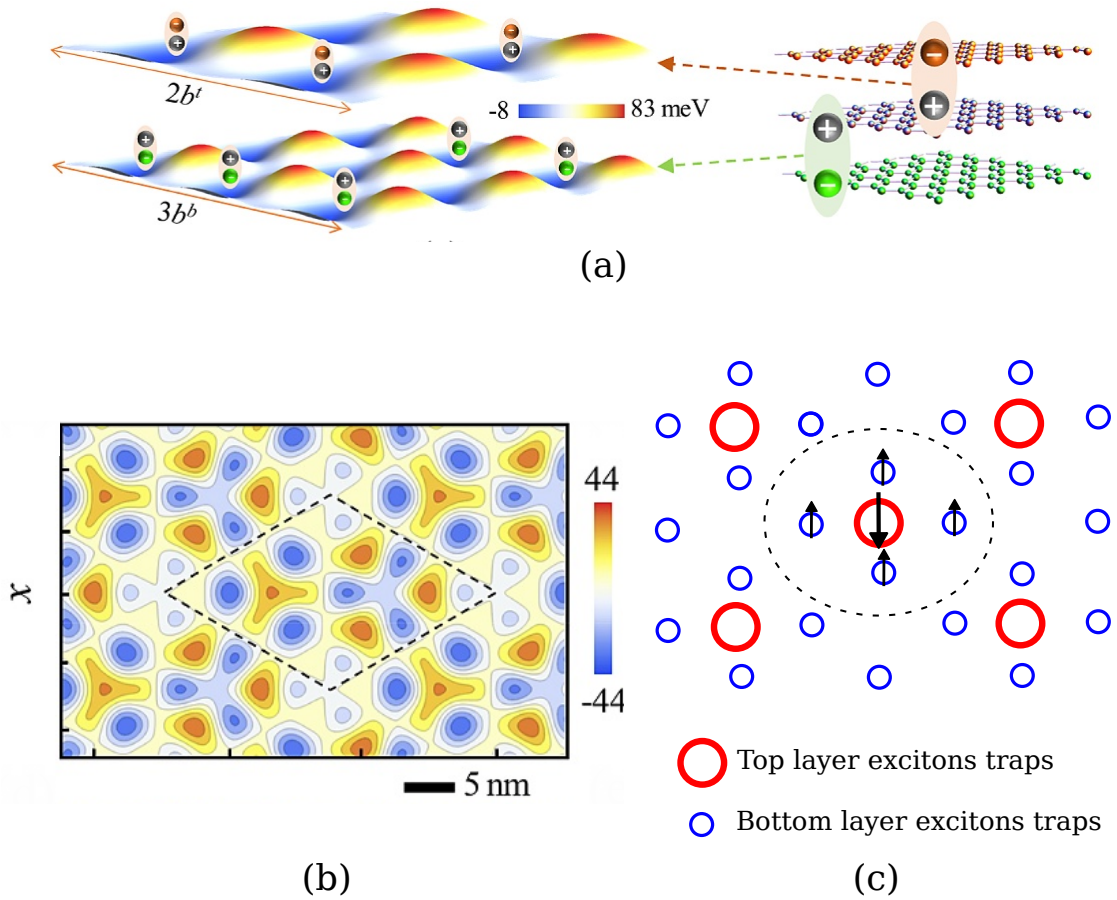

Figure 11: Moiré potentials in TMD trilayers. (a) Combination of moiré potentials results in localized, immobile excitons. (b) Moiré potentials as seen by an electron in bilayer with $\theta = 2^o$. Figures (a) and (b) adapted from reference [30]. (c) Model for moiré traps for top and bottom excitons.

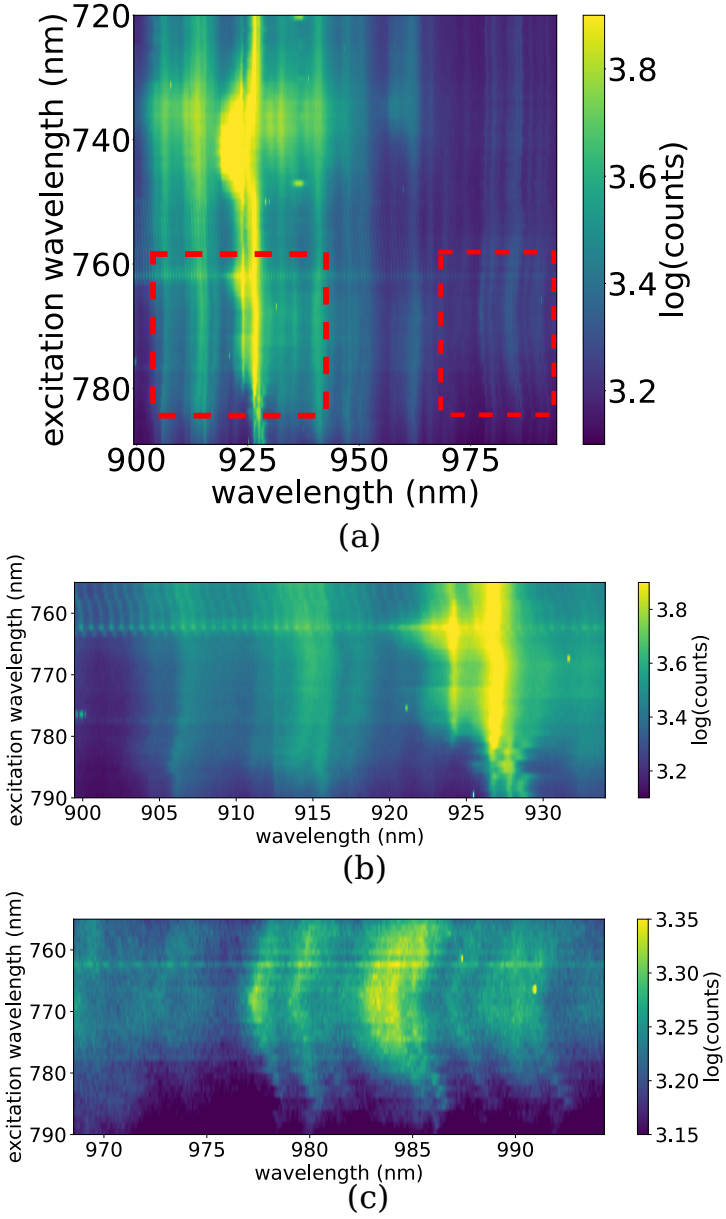

Figure 12: Shift in energy of exciton peaks with excitation wavelength (excitation power=4 μW, integration time=50 s). (a) Bottom exciton blueshift at $MoSe_2$ resonance, causing a red shift in top excitons. Top excitons blue shift at WSe_2 resonance, but there is no change in bottom exciton energy. (b) and (c) show enlarged areas of (a) at $MoSe_2$ resonance.

excitons in moiré potentials is shown in figure 12. During PLE measurements of power-dependent shifting exciton peaks, the excitation wavelength is changed, which results in shifts in energy of exciton peaks (12 (a)). This is because, as the excitation wavelength reaches resonant frequencies of WSe_2 and $MoSe_2$, the exciton occupancy of both top and bottom excitons changes, as the generation rate of excitons is modified by the excitation wavelength. We see that there is both a red shift in top peaks and a blue shift in bottom peaks at $MoSe_2$ resonance, which suggests that the density of bottom excitons has increased such that their interaction is more repulsive. This region is shown in figures 12 (b) and (c). The increase in bottom exciton density results in a red shift in top excitons, as the potential traps of top excitons, despite being more dense, are also surrounded by more bottom exciton traps as shown in 11 (c). This causes an attractive potential as described in our model. However, at WSe_2 resonance we again see a blue shift in energy, this time from the top excitons. This has no observable effect on the energy of bottom excitons, again consistent with the model that the top exciton traps are more sparse, and do not affect the energy of bottom excitons.

4 Conclusions

We have fabricated a heterotrilayer TMD device in which antiparallel dipolar interlayer excitons form and interact. We characterized these dipoles using voltage scans, and show that their energy can be tuned as expected under an electric field. Furthermore, the interactions between these dipoles can be both attractive and repulsive, as predicted by our model for exciton densities in a TMD trilayer. We saw power dependent red and blue shifts in the

energy of interlayer excitons, which are signatures of attractive and repulsive interactions between the dipoles. However, we also found that these shifts in energy were highly dependent on the local potential landscape, as defined by moiré potential of excitons. The largest shift observed in interlayer excitons was around 1.5meV, corresponding to a blue shift in the opposite dipole of around 0.5meV. We also found that there were great differences between samples, with the $MoSe_2 - WSe_2 - MoSe_2$ sample showing more significant shifts than the $WSe_2 - MoSe_2 - WSe_2$ sample.

However, more work needs to be done on the exact effect moiré potential and the confinement of interlayer excitons to more precisely predict and define these shifts in energy. We have analyzed one effect that may provide further insight into the moiré confinement of interlayer excitons, which is the shift in energy of top dipoles vs bottom dipoles as the excitation wavelength changes, causing changes in exciton occupations at resonant frequencies.

5 Outlook

One of the greatest difficulties in this project comes from the exact calculations of exciton densities, due the complicated nature of the lattices and the trapping potentials associated with them. The moiré potentials can be finely tuned by the twist angle between lattices, and one potential future direction of this project is the fabrication of trilayer samples with precisely varying twist angles, to investigate the resulting effect on exciton confinement and the dipolar interactions that arise.

There are also a number of effects that remain unexplored in the current system.

One possibility is the flipping of dipoles with electric fields. At high voltages, the field may become so strong that electrons tunnel between several layers to align the exciton's dipole moment with the electric field. We also expect to see the formation of trions and other bound states in different regions of doping.

Furthermore, it has been suggested that dipolar interactions in TMDs could give rise to new phases of matter within the materials, such as highly ordered lattices due to dipolar repulsion, exciton droplet arrangements due to attractive regimes, and exciton superfluids, which may shed light on previously unexplored quantum many body states [6, 35, 36, 5]. Having shown the existence and tunability of both attractive and repulsive interactions in TMDs, this work is a step towards the discovery of such states of matter.

Finally, it has been suggested that TMDs may have future applications to quantum information due to their valley physics [7]. Interlayer excitons have significantly longer life times, making them more viable for such applications.

References

[1] J. R. Schaibley, H. Yu, G. Clark, P. Rivera, J. S. Ross, K. L. Seyler, W. Yao, and X. Xu, "Valleytronics in 2d materials," *Nature Reviews Materials*, vol. 1, p. 16055, Aug 2016.

[2] B. Zhu, X. Chen, and X. Cui, "Exciton binding energy of monolayer ws2," *Scientific Reports*, vol. 5, p. 9218, Mar 2015.

[3] P. Rivera, J. R. Schaibley, A. M. Jones, J. S. Ross, S. Wu, G. Aivazian, P. Klement, K. Seyler, G. Clark, N. J. Ghimire, J. Yan, D. G. Mandrus, W. Yao, and X. Xu, "Observation of long-lived interlayer excitons in monolayer mose2–wse2 heterostructures," *Nature Communications*, vol. 6, p. 6242, Feb 2015.

[4] W. Li, X. Lu, S. Dubey, L. Devenica, and A. Srivastava, "Dipolar interactions between localized interlayer excitons in van der waals heterostructures," *Nature Materials*, vol. 19, pp. 624–629, Jun 2020.

[5] Y. Slobodkin, Y. Mazuz-Harpaz, S. Refaely-Abramson, S. Gazit, H. Steinberg, and R. Rapaport, "Quantum phase transitions of trilayer excitons in atomically thin heterostructures," *Phys. Rev. Lett.*, vol. 125, p. 255301, Dec 2020.

[6] P. Rabl and P. Zoller, "Molecular dipolar crystals as high-fidelity quantum memory for hybrid quantum computing," *Phys. Rev. A*, vol. 76, p. 042308, Oct 2007.

[7] S. Ren, Q. Tan, and J. Zhang, "Review on the quantum emitters in two-dimensional materials," *Journal of Semiconductors*, vol. 40, p. 071903, jul 2019.

[8] K. S. Novoselov, A. K. Geim, S. V. Morozov, D. Jiang, Y. Zhang, S. V. Dubonos, I. V. Grigorieva, and A. A. Firsov, "Electric field effect in atomically thin carbon films," *Science*, vol. 306, no. 5696, pp. 666–669, 2004.

[9] A. H. Castro Neto, F. Guinea, N. M. R. Peres, K. S. Novoselov, and A. K. Geim, "The electronic properties of graphene," *Rev. Mod. Phys.*, vol. 81, pp. 109–162, Jan 2009.

[10] J. N. Coleman, M. Lotya, A. O'Neill, S. D. Bergin, P. J. King, U. Khan, K. Young, A. Gaucher, S. De, R. J. Smith, I. V. Shvets, S. K. Arora, G. Stanton, H.-Y. Kim, K. Lee, G. T. Kim, G. S. Duesberg, T. Hallam, J. J. Boland, J. J. Wang, J. F. Donegan, J. C. Grunlan, G. Moriarty, A. Shmeliov, R. J. Nicholls, J. M. Perkins, E. M. Grieveson, K. Theuwissen, D. W. McComb, P. D. Nellist, and V. Nicolosi, "Two-dimensional nanosheets produced by liquid exfoliation of layered materials," *Science*, vol. 331, no. 6017, pp. 568–571, 2011.

[11] M.-Y. Li, C.-H. Chen, Y. Shi, and L.-J. Li, "Heterostructures based on two-dimensional layered materials and their potential applications," *Materials Today*, vol. 19, no. 6, pp. 322–335, 2016.

[12] M. Liao, Z. Wei, L. Du, Q. Wang, J. Tang, H. Yu, F. Wu, J. Zhao, X. Xu, B. Han, K. Liu, P. Gao, T. Polcar, Z. Sun, D. Shi, R. Yang, and G. Zhang, "Precise control of the interlayer twist angle in large scale mos2 homostructures," *Nature Communications*, vol. 11, p. 2153, May 2020.

[13] A. David, P. Rakyta, A. Kormányos, and G. Burkard, "Induced spin-orbit coupling

in twisted graphene–transition metal dichalcogenide heterobilayers: Twistronics meets spintronics," *Phys. Rev. B*, vol. 100, p. 085412, Aug 2019.

[14] E. Y. Andrei and A. H. MacDonald, "Graphene bilayers with a twist," *Nature Materials*, vol. 19, pp. 1265–1275, Dec 2020.

[15] Y. Cao, V. Fatemi, S. Fang, K. Watanabe, T. Taniguchi, E. Kaxiras, and P. Jarillo-Herrero, "Unconventional superconductivity in magic-angle graphene superlattices," *Nature*, vol. 556, pp. 43–50, Apr 2018.

[16] S. Manzeli, D. Ovchinnikov, D. Pasquier, O. V. Yazyev, and A. Kis, "2d transition metal dichalcogenides," *Nature Reviews Materials*, vol. 2, Jun 2017.

[17] J. C. Slater and G. F. Koster, "Simplified lcao method for the periodic potential problem," *Phys. Rev.*, vol. 94, pp. 1498–1524, Jun 1954.

[18] S. H. Simon, *The Oxford Solid State Basics / Steven H. Simon.* Oxford: Oxford University Press, first edition. ed., 2013.

[19] W. S. Yun, S. W. Han, S. C. Hong, I. G. Kim, and J. D. Lee, "Thickness and strain effects on electronic structures of transition metal dichalcogenides: 2h-mX_2 semiconductors (m = mo, w; x = s, se, te)," *Phys. Rev. B*, vol. 85, p. 033305, Jan 2012.

[20] D. Le, A. Barinov, E. Preciado, M. Isarraraz, I. Tanabe, T. Komesu, C. Troha, L. Bartels, T. S. Rahman, and P. A. Dowben, "Spin–orbit coupling in the band structure of monolayer WSe2," *Journal of Physics: Condensed Matter*, vol. 27, p. 182201, apr 2015.

[21] G. Wang, A. Chernikov, M. M. Glazov, T. F. Heinz, X. Marie, T. Amand, and B. Urbaszek, "Colloquium: Excitons in atomically thin transition metal dichalcogenides," *Rev. Mod. Phys.*, vol. 90, p. 021001, Apr 2018.

[22] C. Robert, D. Lagarde, F. Cadiz, G. Wang, B. Lassagne, T. Amand, A. Balocchi, P. Renucci, S. Tongay, B. Urbaszek, and X. Marie, "Exciton radiative lifetime in transition metal dichalcogenide monolayers," *Phys. Rev. B*, vol. 93, p. 205423, May 2016.

[23] P. Nagler, G. Plechinger, M. V. Ballottin, A. Mitioglu, S. Meier, N. Paradiso, C. Strunk, A. Chernikov, P. C. M. Christianen, C. Schüller, and T. Korn, "Interlayer exciton dynamics in a dichalcogenide monolayer heterostructure," *2D Materials*, vol. 4, p. 025112, jun 2017.

[24] S. Mahatha, K. Patel, and K. Menon, "Electronic structure investigation of mos 2 and mose 2 using angle-resolved photoemission spectroscopy and ab initio band structure studies," *Journal of physics. Condensed matter : an Institute of Physics journal*, vol. 24, p. 475504, 10 2012.

[25] S. Gao, L. Yang, and C. D. Spataru, "Interlayer coupling and gate-tunable excitons in transition metal dichalcogenide heterostructures," *Nano Letters*, vol. 17, pp. 7809–7813, Dec 2017.

[26] K. Dutta and S. De, "Electrical conductivity and dielectric properties of SiO_2 nanoparticles dispersed in conducting polymer matrix," *Journal of Nanoparticle Research - J NANOPART RES*, vol. 9, pp. 631–638, 05 2007.

[27] A. Srivastava, M. Sidler, A. V. Allain, D. S. Lembke, A. Kis, and A. Imamoğlu, "Optically active quantum dots in monolayer wse2," *Nature Nanotechnology*, vol. 10, pp. 491–496, Jun 2015.

[28] Y. You, X.-X. Zhang, T. C. Berkelbach, M. S. Hybertsen, D. R. Reichman, and T. F. Heinz, "Observation of biexcitons in monolayer wse2," *Nature Physics*, vol. 11, pp. 477–481, Jun 2015.

[29] C. Hubert, Y. Baruchi, Y. Mazuz-Harpaz, K. Cohen, K. Biermann, M. Lemeshko, K. West, L. Pfeiffer, R. Rapaport, and P. Santos, "Attractive dipolar coupling between stacked exciton fluids," *Phys. Rev. X*, vol. 9, p. 021026, May 2019.

[30] Q. Tong, M. Chen, F. Xiao, H. Yu, and W. Yao, "Interferences of electrostatic moiré potentials and bichromatic superlattices of electrons and excitons in transition metal dichalcogenides," *2D Materials*, vol. 8, p. 025007, dec 2020.

[31] M. Koperski, M. R. Molas, A. Arora, K. Nogajewski, M. Bartos, J. Wyzula, D. Vaclavkova, P. Kossacki, and M. Potemski, "Orbital, spin and valley contributions to zeeman splitting of excitonic resonances in MoSe 2 , WSe 2 and WS 2 monolayers," *2D Materials*, vol. 6, p. 015001, oct 2018.

[32] T. Woźniak, P. E. Faria Junior, G. Seifert, A. Chaves, and J. Kunstmann, "Exciton g factors of van der waals heterostructures from first-principles calculations," *Phys. Rev. B*, vol. 101, p. 235408, Jun 2020.

[33] K. L. Seyler, P. Rivera, H. Yu, N. P. Wilson, E. L. Ray, D. G. Mandrus, J. Yan, W. Yao,

and X. Xu, "Signatures of moiré-trapped valley excitons in mose2/wse2 heterobilayers," *Nature*, vol. 567, pp. 66–70, Mar 2019.

[34] H. Yu, G.-B. Liu, and W. Yao, "Brightened spin-triplet interlayer excitons and optical selection rules in van der waals heterobilayers," *2D Materials*, vol. 5, p. 035021, may 2018.

[35] Q. Zhu, M. W.-Y. Tu, Q. Tong, and W. Yao, "Gate tuning from exciton superfluid to quantum anomalous hall in van der waals heterobilayer," *Science Advances*, vol. 5, no. 1, 2019.

[36] A. Kogar, M. S. Rak, S. Vig, A. A. Husain, F. Flicker, Y. I. Joe, L. Venema, G. J. MacDougall, T. C. Chiang, E. Fradkin, J. van Wezel, and P. Abbamonte, "Signatures of exciton condensation in a transition metal dichalcogenide," *Science*, vol. 358, no. 6368, pp. 1314–1317, 2017.